Numerical Simulation of Multiphase Magnetohydrodynamic Flow and Deformation of Electrolyte-Metal Interface in Aluminium Electrolysis Cell

Jinsong Hua[*1], Magne Rudshaug[1], Christian Droste[2], Robert Jorgensen[3], Nils-Haavard Giskeodegard[4]

[1] Dept. of Computational Materials Processing, Institute for Energy Technology, N-2027 Kjeller, Norway

[2] Hydro Aluminium Deutschland GmbH, Primary Metal Technology, 41468 Neuss, Germany

[3] Hydro Aluminium, N-6882 Øvre Årdal, Norway

[4] Hydro Aluminium, N-3908 Herøya Industripark, Norway

[*]Corresponding author:

Dr. Jinsong Hua

E-mail address: jinsong.hua@ife.no

Numerical Simulation of Multiphase Magnetohydrodynamic Flow and Deformation of Electrolyte-Metal Interface in Aluminium Electrolysis Cell

Abstract

A computational fluid dynamics (CFD) based multiphase magnetohydrodynamic (MHD) flow model for simulating the melt flow and bath-metal interface deformation in realistic aluminium reduction cells is presented. The model accounts for the complex physics of the magnetohydrodynamic problem in aluminium reduction cells by coupling two immiscible fluids, electromagnetic field, Lorenz force, flow turbulence and complex cell geometry with large length-scale. Especially, the deformation of bath-metal interface is tracked directly in the simulation, and the condition of constant anode cathode distance (ACD) is maintained by moving anode bottom dynamically with the deforming bath-metal interface. The metal pad deformation and melt flow predicted by the current model are compared to the predictions using a simplified model where the bath-metal interface is assumed flat. The effects of the induced electric current due to fluid flow and the magnetic field due to the interior cell current on the metal pad deformation and melt flow are investigated. The presented model extends the conventional simplified box model by including detailed cell geometry such as the ledge profile and all channels (side, central and cross-channels). The simulations show the model sensitivity to different side ledge profiles and the cross-channel width by comparing the predicted melt flow and metal pad heaving. In addition, the model dependencies upon the reduction cell operation conditions such as anode cathode distance, current distribution on cathode surface and open/closed channel top, are discussed.

Keywords: Aluminium electrolysis; Magnetohydrodynamics; Multiphase flow; Metal heaving; Melt flow; Computational fluid dynamics

1 Introduction

The main industrial process for the production of primary aluminium is based on the Hall-Héroult process. As shown in Figure 1, alumina powder is dissolved into a thin layer of electrolytic bath lying on top of a shallow layer of liquid aluminium (also known as bath and metal layers, respectively). A large electric current is supplied via busbars to the carbon anodes, and flows through the shallow layers of molten salt electrolyte and molten aluminium into a carbon cathode lining, where it is collected by iron collector bars. The dissolved aluminium oxide is reduced at the bath-metal interface to form aluminium droplets which sink to the metal pool at the base of the reduction cell. Due to the high electrical resistivity in the bath layer, substantial Joule heating is generated. Besides maintaining the favourable cell operation temperature for the chemical reactions in the electrolysis process, a large amount of Joule heat is lost to the ambient air. In order to improve the energy efficiency, it is very important to keep the anode cathode distance (ACD) as low as technologically possible to minimize heat production. The technical barrier for lowering ACD is that the interface between the bath and metal layers becomes unstable with respect to its sloshing motion resulted by the coupling effects of electromagnetic and hydrodynamic forces. A quasi-stationary motion of the liquid melts and deformation of the metal pad is also resulted inside the reduction cell. High local velocities in the metal can lead to a weakening of the protecting side ledge which could limit the lifetime of the cell. A too high metal heaving complicates the anode setting process and increases the gross consumption of anodes. Hence, understanding the multiphase magnetohydrodynamic (MHD) flow in the cells and developing a proper tool to predict metal pad heaving and melt flow is of significant importance to improve the cell operation.

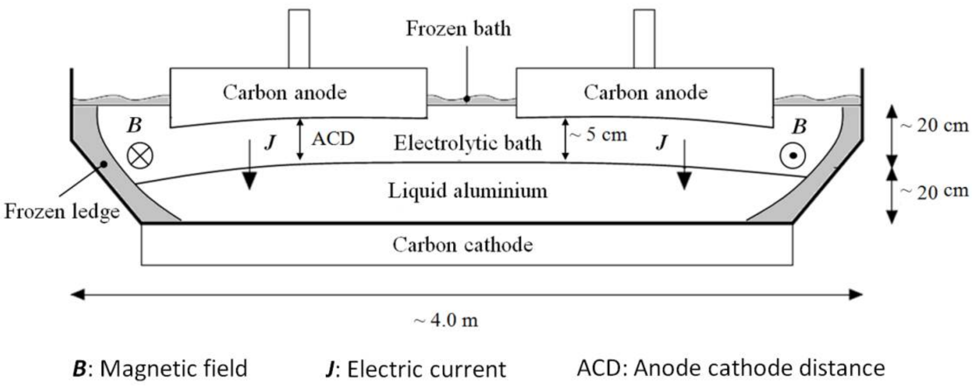

Figure 1: Vertical cut of a Hall-Héroult cell.

Accurate measurements of the melt flow and metal pad deformation in the aluminium reduction cells are hindered by the lack of available precision measuring techniques that can tolerate the high temperature and highly corrosive media. Numerical simulations [1-5] are therefore the most feasible way to study the metal flow pattern and metal pad heaving behaviour, and to investigate the reasons for interface instability. The close coupling between the cell geometry and multiphase MHD flow also brings many challenges for the numerical modelling. A typical industrial aluminium reduction cell has very large aspect ratio (cf. Figure 1) with a width of about 4 m, a metal layer thickness of about 20 cm and a bath layer thickness of about 20 cm. The cell length, depending on the number anodes in the cell, is typically in the range of 10-15 m. The anode is immersed in liquid bath with a small distance (ACD) of typically less than 5 cm away from the top of the metal pad. The anodes are separated from each other and from the ledge by the small channels such as cross-channel, central channel and side channel of several centimetres, The high current flowing in the anodes, the cell interior, the cathodes, and external busbars produces an intense magnetic field (**B**) in both the exterior and the interior of the aluminium reduction cell. The magnetic field interacts with the cell internal electric current (**J**) generating magneto-hydrodynamic (MHD) forces (Lorentz forces). The non-uniform distribution of MHD force leads to melt flow and deformation of the bath-metal interface inside the cell. Due to the heat loss from the side walls of the cell, a layer of frozen ledge is formed. The ledge profile is formed according to the heat balance along the sidewall. Certainly, the ledge profile can affect the electric current density distribution inside the cell and therefore the flow pattern of the liquid melts.

Some simplifications were applied in the previous numerical models for simulating melt flow and metal pad deformation in aluminium electrolysis cells. In the studies by Zikanov et al. [3] and Bojarevics and Pericleous [4], a shallow-water model was used to approximate the bath and metal layers separately. Zikanov et al. [3] neglected the vertical variation in each layer. Only horizontal components of the fluid velocity and the Lorentz force were taken into account. Bojarevics and Pericleous [4] assumed that the vertical momentum equation for a small depth fluid could be reduced to quasi-hydrostatic equilibrium between the vertical pressure and the gravity. The complex effects of realistic cell geometry were simplified. It is clear that the shallow-water model has deficiencies in providing high simulation accuracy and sensitivity for optimizing the aluminium reduction cell design and operation.

Another numerical model category [1, 5] based on technology of computational fluid dynamics (CFD) takes into account the detailed 3D cell geometry and solves the coupled governing equations for turbulent multiphase fluid flow, electromagnetic field and bath-metal interface tracking. Potocnik

[5] made the early trials of using a CFD model to study the bath-metal interface waves in Hall-Heroult cells. The further contributions from Segatz et al. [1] explored more about the possibilities and impacts of CFD modelling for aluminium reduction cell optimization. Severo et al. [6] presented a three-dimensional steady and transient MHD model of aluminium reduction cell by coupling ANSYS and CFX with in-house software. In ANSYS, electrical and magnetic calculations were done with an assumption of a flat metal pad. The calculated electromagnetic force was transferred to CFX, where it was kept constant in the further analysis. Severo et al. [7] compared the performance of different numerical methods (shallow layer method, 3D floating grid method in ESTER/PHOENICS, and 3D VOF method in CFX) to predict the bath-metal interface shape. The complex cell geometry was simplified as a rectangular box with comparable dimensions to a realistic cell. Li et al. [10] reported an inhomogeneous three-phase (bath, metal, gas bubbles) model to predict the melt flow and the bath-metal interface deformation in aluminium reduction cells. Specially, their model took into account the effects of gas bubbles, which were generated under anodes, on the bath flow and the interface stability. The electromagnetic force in the whole fluid region was introduced as a steady source term of the governing equations in the model. Hence, the electromagnetic field was not coupled dynamically with the three-phase model. Recently, a similar modelling approach was also adopted by Wang et al. [13] to understand the effect of innovative cathode geometries (with cylindrical protrusions) on the bath-metal interface fluctuation as well as the energy efficiency in the aluminium electrolytic cell.

To approximate flow physics in a realistic aluminium reduction cell, it is essential to couple the model for multiphase flow and the model for electromagnetic field dynamically. Gerbeau et al. [8] reported a numerical simulation approach for a two-fluid magnetohydrodynamic problem arising in the industrial production of aluminium. The motion of two immiscible fluids was modelled through incompressible Navier-stokes equation coupled with Maxwell equations. An arbitrary Lagrangian-Eulerian formulation was used for moving the interface between the two immiscible fluids. Numerical test cases demonstrated the capability of the nonlinear and fully coupled method to simulate complex MHD phenomena. Munger and Vincent [9] presented another approach for simulating magnetohydrodynamic-instability in aluminium reduction cells. It combined a three-dimensional finite-volume method for incompressible fluid flows based on Navier-Stokes equation, a level set technique to track the interface movement, and an electromagnetic model for the evolution of electric and magnetic fields. The feasibility of the numerical methods in [8, 9] was demonstrated through some test cases with simplified cell geometry, but it was not tested for a model with the dimensions of a realistic reduction cell.

CFD based multiphase MHD flow models have been used for improving cell design and operation efficiency. Das et al. [11, 12] presented a mathematical model for investigating the magnetohydrodynamic (MHD) effects in aluminium reduction cell using finite element method. Their study focused on the distribution of electromagnetic force and electric current density. Especially, they focused on the effects of the inclination of cell side walls and the cathode collector bar material. In their model, the bath-metal interface was assumed to be flat. Recently, Song et al. [14] used a multiphase MHD flow model to study the impact of cathode material and shape on current density distribution in aluminium reduction cell. The geometry of cathode top was modified to improve the uniformity of current density, lower the metal flow speed and stabilize the bath-metal interface to reduce energy consumption.

The new model presented in the following is an attempt to accurately and efficiently predict the melt flow and metal pad heaving in aluminium reduction cells with realistic geometry based on the dynamically-coupled two-phase MHD flow model developed by Hua et al. [15, 16]. This model coupled effects of the electric potential/current distribution, the melt flows in the bath and metal layers, the interface deformation, and the anodes at a constant distance to the metal interface. The model of [15] was based on a rectangular box geometry. Although the details of all channels (side, end, central and cross-channels) were taken into account, the effect of a ledge profile was however ignored. By using this simplification, the model deviates from the situation for realistic aluminium reduction cells. To overcome this deficiency, the model of [15] was extended further in the development of [16] with the capability to account for the effect of a realistic ledge profile so that the model can be used for studying realistic aluminium reduction cells.

In this paper, the fundamentals of the multiphase MHD model are presented in Section 2. After this, the model is applied to a hypothetical aluminium reduction cell with realistic cell geometry and operational conditions. The governing transient equations for turbulent multiphase flow, interface tracking and electromagnetic fields are solved fully coupled on one common platform: ANSYS Fluent. The simulation starts with a stationary flow field and flat bath-metal interface with a fixed current density distribution on the cathode as boundary condition and a background magnetic flux density field in the whole solution domain. The electromagnetic force (the Lorentz force) field distribution is calculated at each time step. The electromagnetic model can take into account the induced current due to the movement of conductive fluid in a magnetic field, the induced magnetic field due to the electric current flowing within the reduction cell, and the deformation of the bath-metal interface. The detailed information about the cell geometry and cell operation conditions of a hypothetical aluminium reduction cell is described in section 3. Initially the anode bottom is flat, but updated dynamically keeping a constant distance from the deforming bath-metal interface to ensure realistic operational conditions of an aluminium reduction cell. The simulation results are presented in Section 4, where the model sensitivity to cell geometry and operation conditions are analysed and discussed. This is achieved by comparing the simulation results of melt flow pattern and metal pad heaving of a reference case with those of the test cases through varying model settings, cell geometry and boundary conditions. To test the model performance, the effects of the model settings with flat bath-metal interface, the inclusions of the induced current density and the induced magnetic field are studied. In order to understand the effects of side ledge and cross-channel, simulations with different ledge profiles and cross-channel widths were conducted and the predictions on metal pad heaving and flows are compared. In addition, the sensitivity of the results on ACD, current density distribution on cathode and open channel top is discussed.

2 Fundamentals and model implementation

The multiphase MHD flow model is developed and implemented on the platform of a commercial CFD tool package ANSYS Fluent. By using the so called User Defined Functions (UDF), the coupling among two-phase liquid flow, interface deformation, magnetic flux density, electrical potential, current density distribution and the Lorentz force is realized.

2.1 Governing equations for melt flow

The two-phase VOF model in ANSYS Fluent is used for solving the governing equations for flow fields and tracking the interface deformation. The governing equations of continuity and momentum conservation of the two-phase flow system with incompressible fluids read,

$$\nabla \cdot \mathbf{u} = 0 \tag{1}$$

$$\frac{\partial}{\partial t}(\rho \mathbf{u}) + \nabla \cdot (\rho \mathbf{u}\mathbf{u}) = -\nabla P + \nabla \cdot \left[\mu\left(\nabla \mathbf{u} + \nabla \mathbf{u}^T\right)\right] + \mathbf{F}_E + \rho \mathbf{g} \tag{2}$$

where $\mathbf{u}$ represents the flow field, and P is the pressure. The gravitational acceleration is **g,** and $\mathbf{F}_E$ the electromagnetic force, which is calculated by the electromagnetic model described in section 2.3. The fluid density and viscosity are given by ρ and μ respectively. For a two-fluid system, the fluid properties are calculated with weighted averaging of each phase volume fraction,

$$\rho = \rho_1\alpha_1 + \rho_2\alpha_2 \tag{3}$$

$$\mu = \mu_1\alpha_1 + \mu_2\alpha_2 \tag{4}$$

where the subscripts 1 and 2 denote the primary phase and the secondary phase respectively, and α the fluid volume fraction. In the present model, the bath is set as the primary phase, and the metal as the secondary phase.

2.2 Governing equations for bath-metal interface tracking

The VOF method in ANSYS Fluent is used to obtain the distribution of each phase volume fraction and to track the phase-interface deformation. The continuity of the secondary phase is obtained by solving the governing equation for the phase volume fraction α_2,

$$\frac{\partial \alpha_2}{\partial t} + \mathbf{u} \cdot \nabla \alpha_2 = 0 \tag{5}$$

The primary-phase volume fraction (α_1) will be determined by the phase continuity constraint: $\alpha_1 = 1 - \alpha_2$.

2.3 Governing equations for electromagnetic field

The electric current in the aluminium reduction cell (**J**) is calculated from Ohm's law taking into account the effect of the induced current ($\mathbf{J}_{ind}$) due to the flowing conductive liquid in a magnetic field (**B**),

$$\mathbf{J} = \sigma\mathbf{E} + \mathbf{J}_{ind} \quad \text{and} \quad \mathbf{J}_{ind} = \sigma(\mathbf{u} \times \mathbf{B}) \tag{6}$$

where σ is the electrical conductivity of liquid, $\mathbf{E}$ is the electric field intensity, and $\mathbf{B}$ is the magnetic flux density. The electric field intensity can be expressed in terms of electrical potential (φ) as $\mathbf{E} = -\nabla\varphi$. The charge conservation principle ($\nabla \cdot \mathbf{J} = 0$) gives the governing equation for electric potential as

$$\nabla \cdot \sigma\nabla\varphi = \nabla \cdot \mathbf{J}_{ind} = \nabla \cdot [\sigma(\mathbf{u} \times \mathbf{B})] \tag{7}$$

A volume fraction weighted harmonic average method is mandatory to calculate the distribution of electrical conductivity,

$$\frac{1}{\sigma} = \frac{\alpha_1}{\sigma_1} + \frac{\alpha_2}{\sigma_2} \tag{8}$$

So, the distribution of the electrical conductivity field in the fluid is varied as the bath-metal interface deforms.

A user defined scalar equation on the ANSYS Fluent platform is set up to solve the governing equation (7) for electric potential distribution inside the reduction cell. The electric current density inside the cell can be calculated as,

$$\mathbf{J} = -\sigma \nabla\varphi + \sigma(\mathbf{u} \times \mathbf{B}) \tag{9}$$

The magnetic field is calculated using steady-state Maxwell's equations,

$$\nabla \cdot \mathbf{B} = 0, \tag{10}$$

$$\nabla \times \mathbf{H} = \mathbf{J}_t, \tag{11}$$

$$\mathbf{B} = \eta \cdot \mathbf{H}, \tag{12}$$

where $\mathbf{H}$ is the magnetic field intensity and η the magnetic permeability of fluid. $\mathbf{J}_t$ is the total electric current including both the current flowing inside the reduction cell ($\mathbf{J}$) and the electric current in the external busbar system ($\mathbf{J}_o$). In virtue of Helmholtz's theorem, the magnetic vector potential ($\mathbf{A}$) can be defined uniquely by

$$\nabla \times \mathbf{A} = \mathbf{B}. \tag{13}$$

The governing equation for magnetic vector potential ($\mathbf{A}$) can be reformulated as,

$$\nabla^2 \mathbf{A} = -\eta \mathbf{J}_t. \tag{14}$$

Inside aluminium reduction cells, a large part of the magnetic field is given by the electric current in the busbar system ($\mathbf{J}_o$). This part of magnetic field is also known as background magnetic flux density field ($\mathbf{B}_o$). Since the aluminium reduction cell is the focus of the current study, the busbar system is neglected. The background magnetic flux density field is given analytically to simplify the benchmarking. It is based on a least square fitting of results calculated by an in-house electromagnetic model which includes the busbar system. The magnetic field is also partly given by the electric current inside the aluminium reduction cell. The magnetic vector potential ($\mathbf{A}_i$) for the induced magnetic field ($\mathbf{B}_i$) can be obtained by solving the following equation

$$\frac{1}{\eta}\nabla^2 \mathbf{A}_i = -\mathbf{J} = \sigma\nabla\varphi - \sigma(\mathbf{u} \times \mathbf{B}). \tag{15}$$

with the boundary values ($\mathbf{A}_b$) by Biot-Savart law

$$\mathbf{A}_b = \frac{\eta}{4\pi}\int_V \frac{\mathbf{J}}{R}\,dv. \tag{16}$$

where R is the distance between the boundary point and the mesh elements inside the integration domain, the whole volume V of the reduction cell. The induced magnetic flux density field ($\mathbf{B}_i$) can be calculated from the magnetic vector potential ($\mathbf{A}_i$) from equation (15) as,

$$\mathbf{B}_i = \nabla \times \mathbf{A}_i. \tag{17}$$

The total magnetic flux density field inside the aluminium reduction cell can be calculated as,

$$\mathbf{B} = \mathbf{B}_o + \mathbf{B}_i. \tag{18}$$

The electromagnetic force (Lorentz force) density is given as

$$\mathbf{F}_E = \mathbf{J} \times \mathbf{B}, \tag{19}$$

2.4 Turbulence model

To simulate the melt flow in a realistic reduction cell with dimensions about 10 m in length and 4 m in width, a proper turbulence model is necessary. To limit the complexity of the problem, the standard k-ε turbulence model with standard wall functions is used to calculate the turbulent viscosity in the each phase. Our numerical exercises [15, 16] indicate that the standard k-ε turbulence model makes reasonable predictions with relatively coarse meshes, which shortens the total calculation time required for the transient simulation of the metal pad profile development in the aluminum electrolysis cells. The deficiencies of the k-ε turbulence model for such type of flow, where recirculation and re-attachment could occur at the boundary layer, are well known (cf. Pope [17]). Alternative, e.g. k-omega model, could be a better choice, but ultimately require an exceedingly fine meshing for the boundary layer and long calculation time for the current application.

3 Model description and realistic reference model

3.1 CFD model

The overall geometry of an aluminium reduction cell is shown in Figure 2(a). It has a length of 11.6 m and a width of 3.9 m. The thickness of the metal layer is 0.24 m, and that of the bath layer is 0.21 m. The ACD is set to be 0.04 m. The aluminium reduction cell consists of thirty anodes in total. Each anode has the dimensions of 0.704 m × 1.61 m in the horizontal directions. The width of central channel and cross-channels is 0.2 m and 0.04 m, respectively. The width of the end- and side-channels is now defined by the ledge profiles which are given in section 3.4.

A structured mesh of hexahedral cells is used for the CFD model as shown in Figure 2(b). In the horizontal directions, the central channel and side channel are meshed with four mesh cells, the cross-channel is meshed with two mesh cells, and each anode is meshed with 20×12 cells. In the vertical direction, the model is divided into three zones. The top zone covering the bath layer above the anode bottom is meshed with twelve cells. The middle zone is the interface deformation zone. It has a thickness of 0.26 m which covers the ACD zone and part of metal layer. It is meshed with eighteen cells with fine meshes to capture the interface deformation. The bottom zone, which has a height of 0.086 m, is meshed with ten mesh cells. The CFD model contains 305216 hexahedral cells in total. The selection of hexahedral cell is based on our experience that larger aspect ratio with large dimension in the horizontal directions and small dimension in the vertical direction is tolerated in the simulations. Good simulation accuracy can be obtained with fewer elements, which ultimately speeds up the simulations.

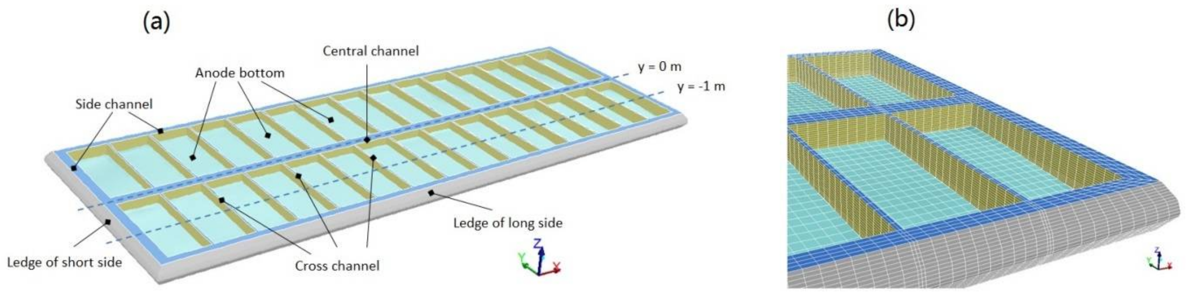

Figure 2: (a) An overview of the model for a realistic reference alumina reduction cell, (b) a zoom view of the CFD model about ledge profile and deformed anode bottom.

3.2 Strategy for maintaining constant ACD

In the realistic cell operation, the anode bottom positon and anode current pick-up are affected by at least two basic mechanisms: (1) the vertical positions of all anodes are adjusted mechanically by an

ACD controlling system which moves all anodes at the same time up or down by the same distance regulating the cell voltage; (2) the individual anode bottom is burned off in the electrolysis process depending on the distance to the metal surface. In the present model, a quasi-static situation is considered a couple of hours after the last anode movement (mechanism (1)) where all anode bottoms have the same distance to the metal by the burn-off mechanism (mechanism (2)).

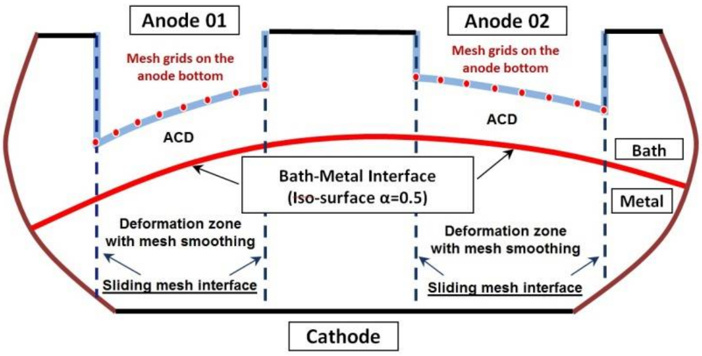

Figure 3: Modelling strategy to maintain constant anode cathode distance (ACD) by relocating the anode bottom mesh grids according to the deformed bath-metal interface.

Significant efforts have been put on developing the model capability to ensure a constant ACD based on the calculated metal heaving as shown in Figure 3. We implement this in ANSYS Fluent by applying the sliding mesh feature. Vertical sliding mesh interfaces between the region under the anodes and the region under the channels are created. The meshes on both sides of the sliding mesh interfaces may be non-conformal, and the fluid flow data on one side of the interface can be interpolated from the other side to ensure continuity. To mimic the anode consumption, the vertical position of each anode bottom grid has to be adjusted according to the bath-metal interface height. Following the anode bottom grid adjustment, the connected mesh in the neighbouring region under the anodes is deformed accordingly, known as the mesh deformation zone. To maintain reasonably good mesh quality in this mesh deformation zone, mesh smoothing technique is adopted as well. To implement the above described modelling strategy, ANSYS Fluent UDFs has been developed to calculate the vertical distance between the bath-metal interface and the anode bottom at each time step.

The ability to maintain a constant ACD provides a better approximation to the operation of realistic aluminium reduction cells. Especially, when modelling high energy efficient reduction cells with small ACD, the overall deformation of bath-metal interface can be larger than ACD and it may touch the anode bottom during the simulation if the anode bottom is kept fixed. This makes the model deviate from the situation of actual cell operation, and may lead to simulation divergence.

3.3 Material properties

In the CFD model setup, the material properties for the fluids, electrolyte and liquid aluminium are required; they are summarized in Table 1.

3.4 Boundary conditions

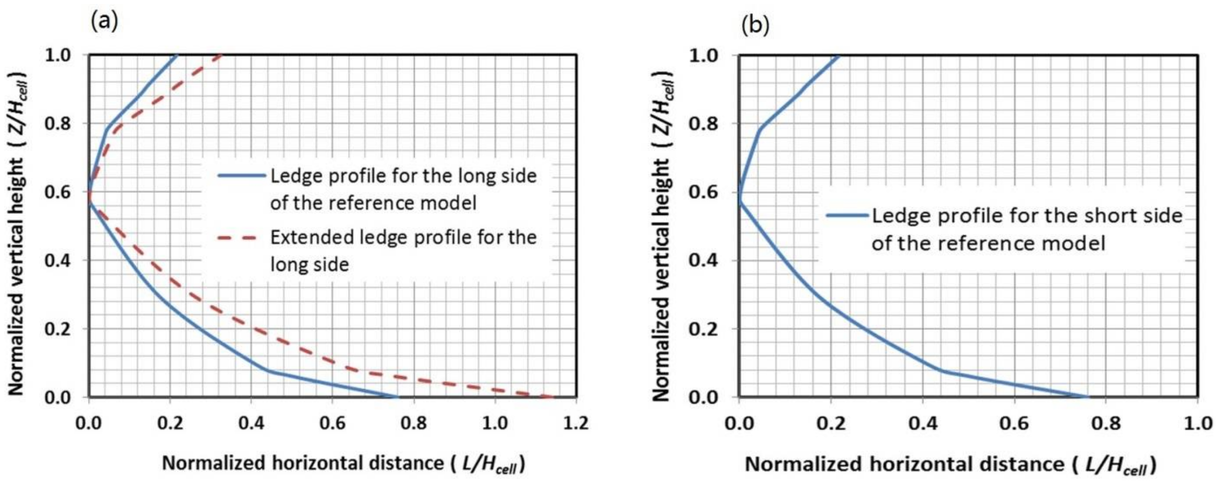

Figure 4: (a) Ledge profiles for the long side of the reference model and for a test model to investigate its significance; (b) Ledge profile for the short side of the reference model.

In order to simplify the cell geometry a rectangular box was used in the CFD models of [7, 15] to simulate the melt flow and bath-metal interface deformation in aluminium reduction cells. The study of Das et al. [11] indicated that the direction of Lorentz force is significantly influenced by the slope of the cell side walls and is important to convective flow of metal and bath inside the cell. Actually, the ledge profile is dynamic and changes during cell operation. In order to make the current CFD model resemble the realistic aluminium reduction cell more closely, the ledge profile due to frozen alumina on the cell walls should be taken into account. Figure 4 shows two normalized side ledge profiles introduced in this paper to study the effects of side ledge profile on bath and metal flow fields and metal pad heaving. Here, the side ledge profile is normalized with respect to the cell height, the total thickness of bath and metal layers. One ledge profile is used for the reference model, and the extended ledge profile is used to study model sensitivity. The ledge profiles are based on the analysis results of an in-house ledge profile code.

For fluid flow, no slip boundary conditions are applied on all solid wall surfaces. The free surface on the channel top is simplified as slip boundary with zero shear stress. Standard wall functions are assumed on all solid walls for solving the k-ε turbulence model.

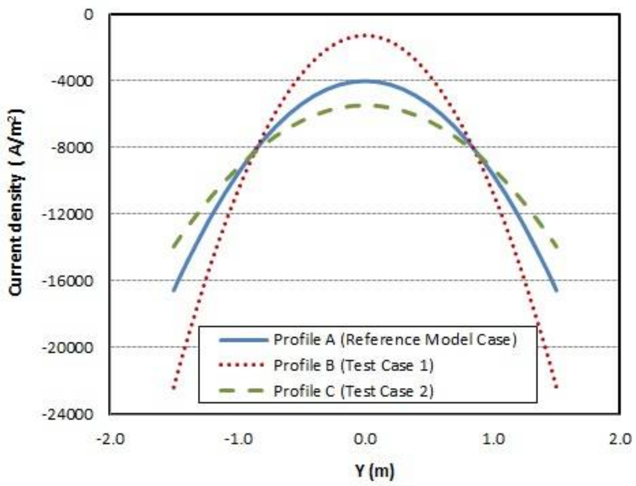

Figure 5: Electric current density profiles on the cathode surface.

As for the boundary conditions for the electric potential equation, zero electric potential is set on anode bottom and anode sides. Electric insulation conditions are applied on the cell side walls and the channel top, where the normal current density is set zero. Three profiles of normal current density (A/m^2) on the cathode surface as shown in Figure 5 are assumed for different test cases,

$$J_z^A = J_k(-4016-5577Y^2)\,. \tag{21}$$

$$J_z^B = J_k(-1286-9374Y^2)\,. \tag{22}$$

$$J_z^C = J_k(-5475-3764Y^2)\,. \tag{23}$$

where J_k is a scalar factor with unit A/m^2, which ensures that the total current on cathode matches the cell amperage 300 kA for the simulation tests with different ledge profiles. Y is the normalized coordinate $Y = y/L_0$, where L_0 is the length scale unit L_0 = 1 m. The origin of the coordinate system is located at the centre of cell bottom. The normal current density profile J_z^A is used for the reference model and the normal current density profiles J_z^B and J_z^C for sensitivity study. The assumptions of the current density distribution profiles are based on the analysis results of an in-house electromagnetic model and our experience from realistic cell operations. Similar current density profiles can also be found in [7] for the benchmark study case.

The background magnetic field ($\mathbf{B}_o$) imposed upon both bath and metal layers inside the reduction cell is assumed as,

$$\begin{cases} B_x = B_k\left(-1.5 - 0.2X + 8.0Y\right) \\ B_y = B_k\left(-0.7 - 1.0X + 0.2Y\right) \\ B_z = B_k\left(-0.02 - 0.1X - 0.5Y - 0.7XY\right) \end{cases} \tag{24}$$

where B_k is the magnetic flux density scale in unit mT. The normalized coordinate $X = x/L_0$. It is assumed that the background magnetic field has no dependence upon the vertical coordinate Z. This is a best fitted correlation upon the result of an in-house magnetic field model for realistic aluminium reduction cells. The background magnetic field ($\mathbf{B}_o$) shows the main characteristics of those seen in realistic aluminium reduction cells where only the busbar system is included.

The initial fluid flow field inside the reduction cell is assumed to be stationary. The bath-metal interface is initialized as a flat horizontal surface with an ACD of 0.04 m under the anode bottom. The initial electric potential is set to zero everywhere.

3.5 Solution method

General numerical schemes provided by ANSYS Fluent were applied: "SIMPLE" for pressure-velocity coupling, the spatial discretization scheme "PRESTO!" for pressure, the "Geo-Reconstruct" scheme for volume fraction, and "First Order Upwind" for other equations. Transient simulation is adopted. "First Order Implicit" scheme is applied for the transient formulation. The time step size is set to constant as 0.04 s. The steadiness of the transient simulation results is estimated by averaging the transient data over a certain period of 4 s. It is found that the simulations reach quasi-steady state after 200 s simulation time (5000 time steps).

4 Results and discussion

4.1 Results of realistic reference model

A reference model is set up to study the model sensitivity through varying the model settings. For the reference model, the induced current density due to a flowing conductive liquid in magnetic field is ignored ($\mathbf{J}_{ind} = 0$), and the induced magnetic flux density field due to the current flowing inside the cell is neglected ($\mathbf{B}_i = 0$). The ledge profiles for the reference model are shown in Figure 4. The normal electric current density profile on the cathode surface for the reference model (Profile A) is shown in Figure 5.

The temporal variations of the metal pad height and the flow pattern on the metal pad for the reference reduction cell are shown in Figures 6 and 7, respectively. Just 20 s after the start of the simulation, the bath-metal interface, as shown in Figure 6(a), significantly heaves at the cell centre, and sinks at the four corners of the reduction cell. The heaving amplitude of metal pad varies slightly along the short axis of the cell, but the metal pad height varies significantly along the long axis of the cell. The corresponding flow pattern on the bath-metal interface is shown in Figure 7(a). Certainly, the circulating melt flows at the corners of the reduction cell also contribute to lower the bath-metal interface at the centres of the vortices as shown in Figures 7(b), (c) and (d),

As the melt flow develops inside the reduction cell, several vortices are induced at the cell centre. As a result, the bath-metal interface is adjusted accordingly. A dome-shaped metal pad is formed inside the aluminium reduction cell as shown in Figures 6(b), (c) and (d). Finally, both the flow pattern of the melt on the bath-metal interface (shown in Figures 7(e) and (f)) and the metal pad heaving (shown in Figures 6(e) and (f)) reach a quasi-steady state with minor changes with time.

In real cell operation, the process from the starting to the steady operation may take hours or even days, which is longer than the initial period about 100 s shown in the simulation. This deviation is due to the lack of proper sub-models for anode burn-off mechanism and anode movement mechanically by the ACD controlling system, especially for the cell start-up process. To mimic the anode movement and bottom profile development, the anode bottom is adjusted according to the bath-metal interface height to keep a constant ACD. This modelling method provides us with a quick and reliable transition period from the initial stationary flow field with a flat bath-metal interface to the quasi-steady state flows with significant metal pad heaving in the simulations. Certainly, our interest is put on the predictions of the metal pad heaving and the melt flows at the quasi-steady state, not in the transition period. The predicted behaviour in the transition period can only provide us with some hints about the mechanism of developing the metal pad heaving and the melt flow patterns.

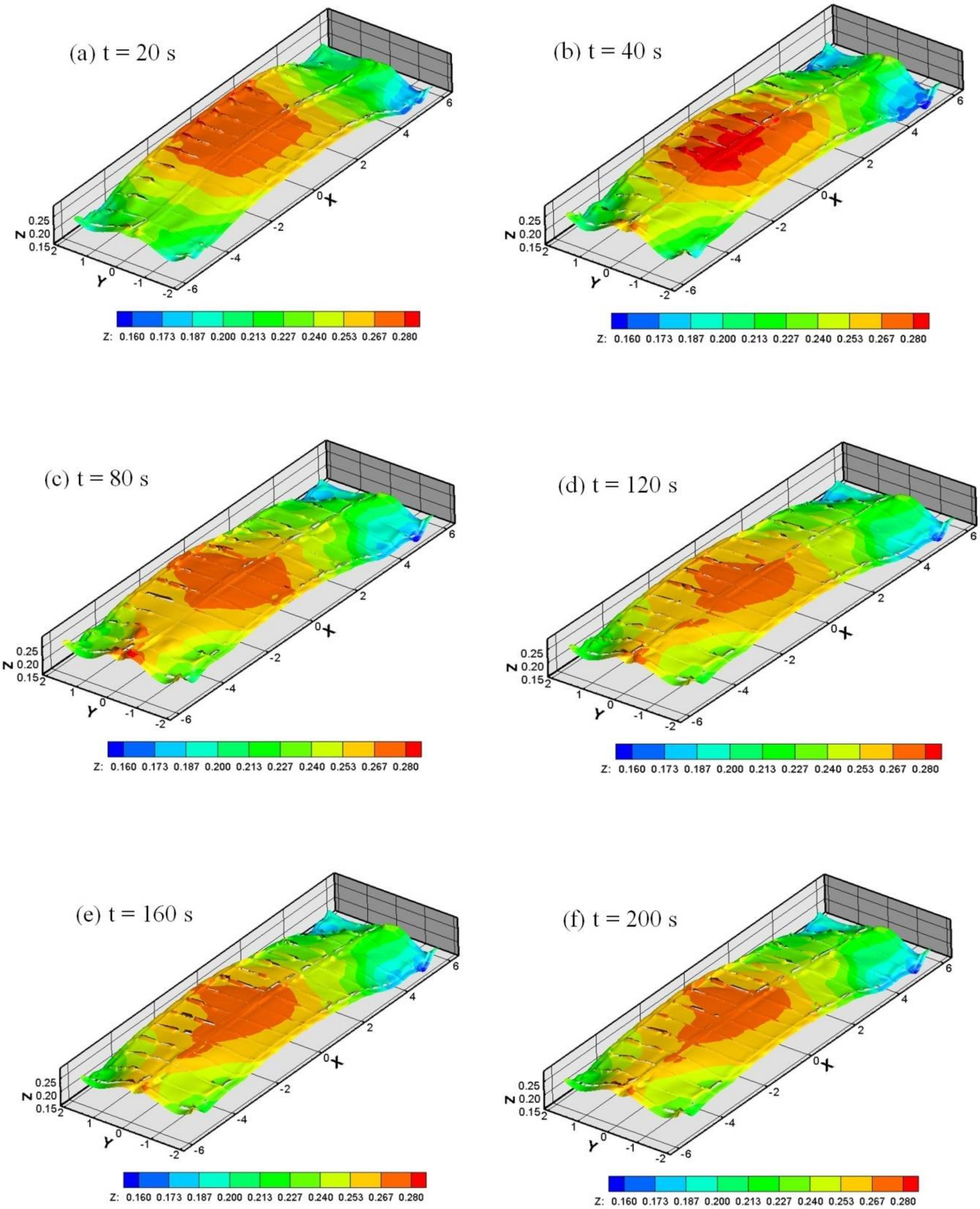

Figure 6: Predicted temporal variation of bath-metal interface height for the reference aluminium reduction cell.

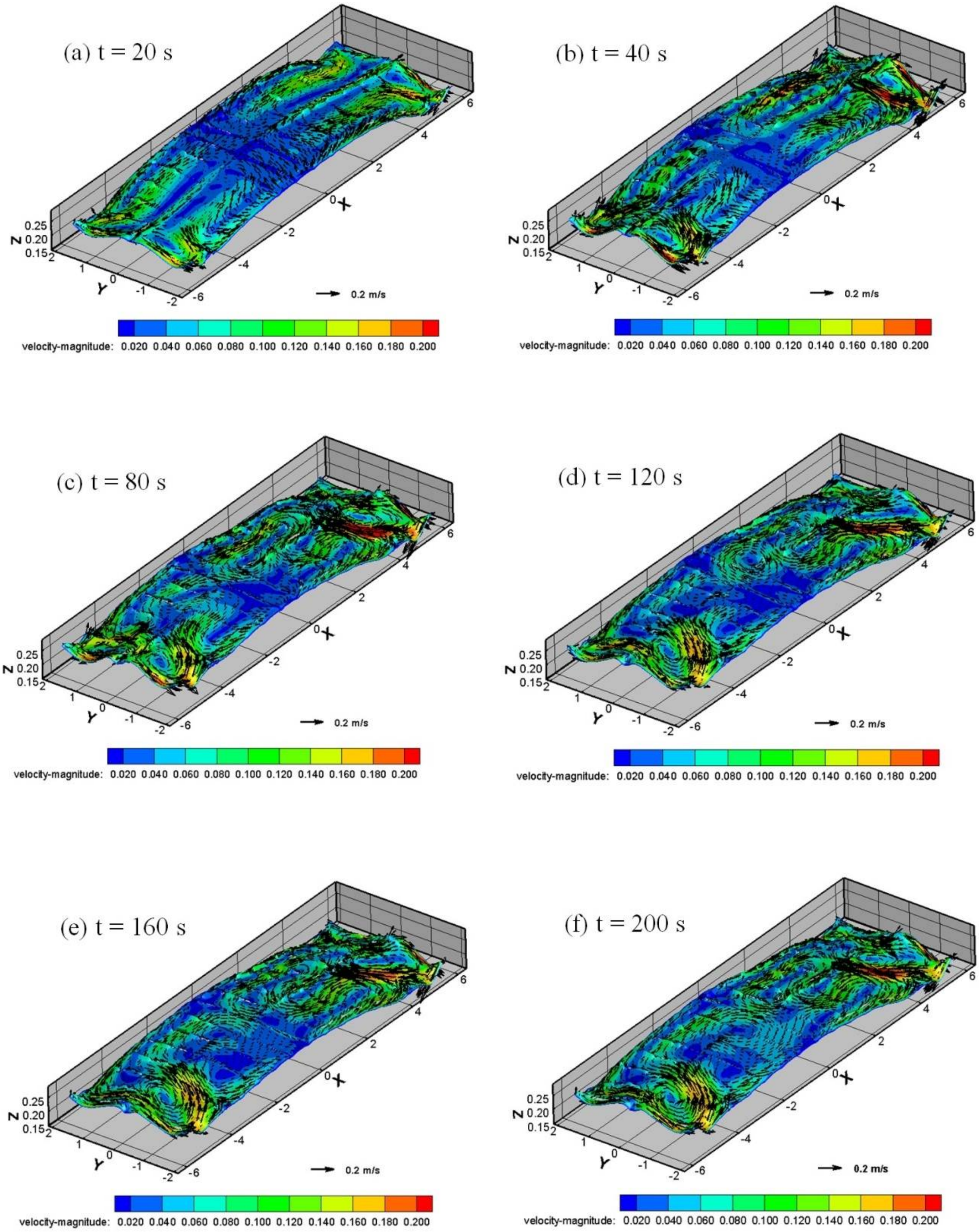

Figure 7: Predicted temporal variation of flow pattern on the bath- metal interface for the reference aluminium reduction cell.

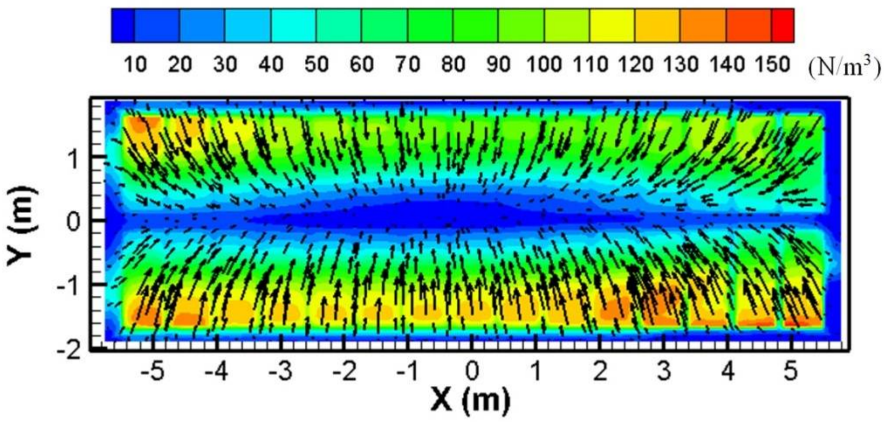

Figure 8: Distribution of Lorentz force on the horizontal plane Z= 0.2m at the quasi-steady state.

Figure 8 shows the distribution of electromagnetic force on the horizontal plane z = 0.2 m at the quasi-steady state. The vectors of Lorentz force point from the cell sides to the centre. The magnitude of the Lorentz force is smaller at the cell centre and larger at the cell sides. It is believed that the irrotational part of the electromagnetic force is the dominating cause of the metal pad heaving before the flow pattern is built up inside the reduction cell. Under the effect of the electromagnetic forces, circulating flows are started at the four corners of the reduction cell, and a quasi-steady state circulating melt flow and bath-metal interface deformation can be obtained eventually.

The simulation results for the reference cell model indicate that the maximum difference of metal pad height (metal pad heaving) is about 0.13 m, and maximum velocity on the bath-metal interface is about 0.22 m/s. These are typical values for realistic reduction cells under similar operating conditions.

4.2 Model with assumption of flat bath-metal interface

In several previous numerical models [11], for aluminium reduction cells, the bath-metal interface is assumed to be flat when calculating the melt flow under the effect of an electromagnetic force. The pressure head distribution on the flat interface is then used to estimate the metal pad deformation (H_{mpd}) inside the reduction cell as,

$$H_{mpd} = \frac{p}{g\left(\rho_{metal} - \rho_{bath}\right)}. \tag{25}$$

In order to understand the difference caused by the assumption of flat interface in the modelling, we conduct a simulation test case which freezes the bath-metal interface at its initial position, and the simulation results are compared with those of the reference model. The predicted quasi-steady state liquid flow on the flat interface is shown in Figure 9(a). When it is compared with the predictions of the reference model shown in Figure 7, the overall liquid flow pattern on the interface is quite different. The maximum liquid flow magnitude predicted by this model is higher than that by the reference model. The circulating liquid flows at the long ends of the reduction cell are predicted by both models. The estimated metal pad deformation is shown in Figure 9(b). When it is compared to the predicted bath-metal interface height distribution obtained by the reference model, both models predict the metal pad heaving at the cell centre, however the heaving profiles are quite different. By comparing the model predictions, it can be concluded that the assumption of a flat bath-metal interface [11] can result in significant deviations compared to the model without this assumption.

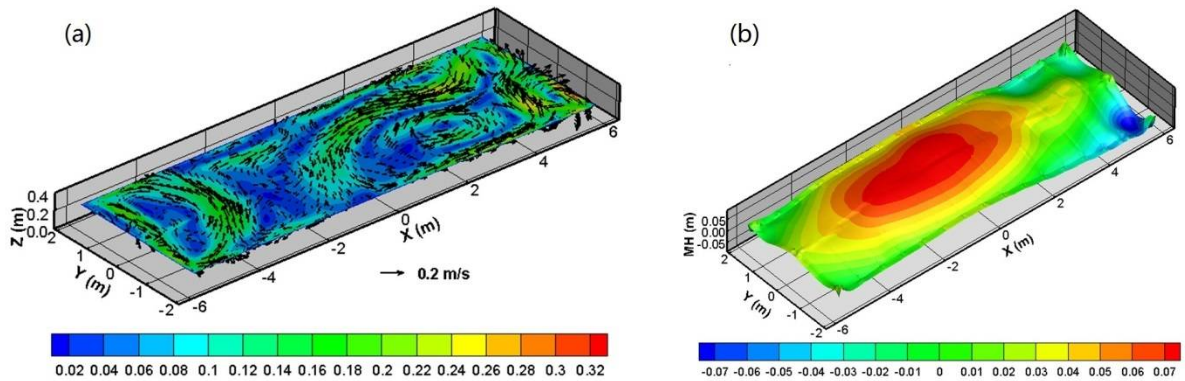

Figure 9: (a) Predicted flow pattern on the bath-metal interface and (b) estimated metal pad heaving for an aluminium reduction cell model with the assumption of flat bath-metal interface.

4.3 Effect of flow induced electric current

In order to investigate the effect of induced electric current, a simulation is conducted based on the basic settings of the reference model except that the setting for the induced electric current, due to conductive liquid flowing in magnetic field, is turned on. At the quasi-steady state, the model prediction of the total current distribution on a horizontal plane ($z = 0.1$ m) in the metal layer is shown in Figure 10(a), and the induced current distribution in Figure 10(b). The high magnitude of induced electric current occurs at the two longitudinal ends of the reduction cell, where the liquid flows at high speed. The induced electric current density magnitude is about one third of the total electric current locally, which contributes significantly to the current density distribution in the reduction cell. The predicted bath-metal interface height distribution and the flow pattern are shown in Figure 11. Compared with predictions of the reference model, they are quite similar. Detailed comparisons of the metal pad deformation (averaged from t = 140 s to t = 200 s) along the cell central channel (y = 0 m) and the cell long side section (y = -1.0 m) predicted by the current model and the reference model are shown in Figure 12. The induced electric current does not affect the overall metal pad deformation, but does affect the metal pad deformation at both longitudinal ends of the reduction cell.

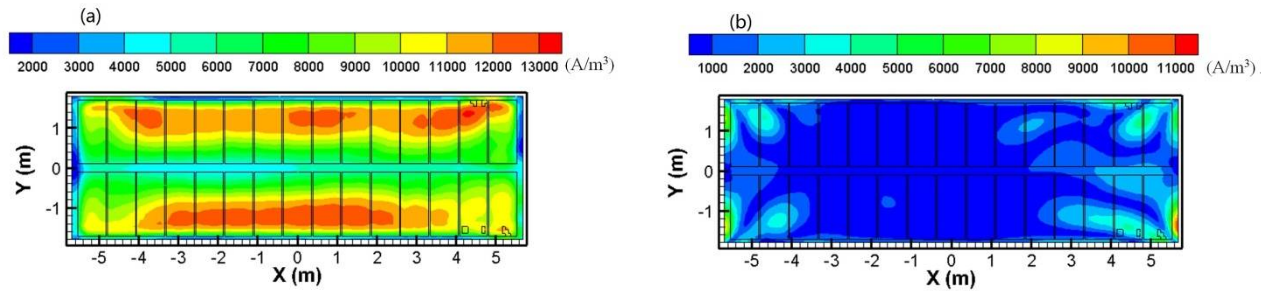

Figure 10: Distributions of (a) total current magnitude and (b) flow induced electric current magnitude at the horizontal plan of z = 0.1m at the quasi-steady state.

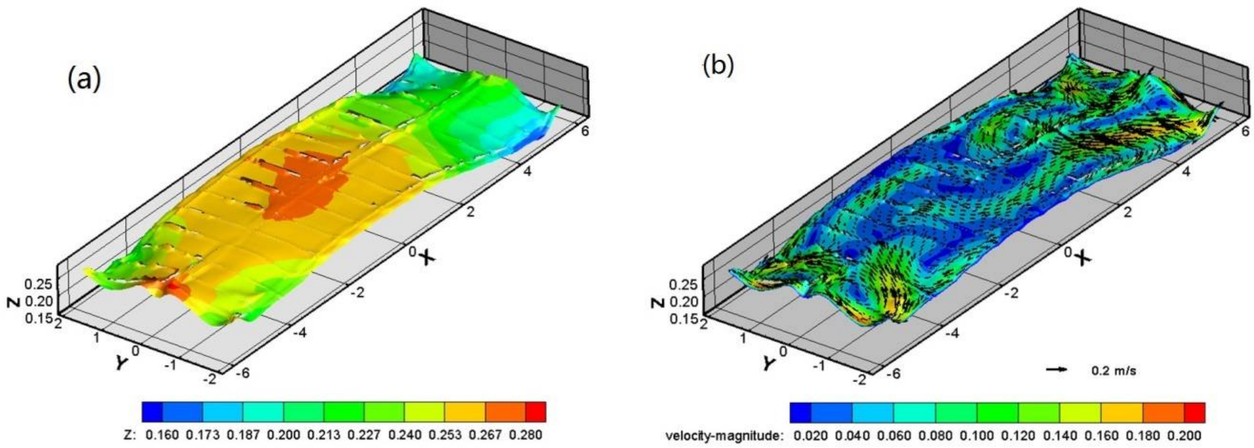

Figure 11: Predicted (a) bath-metal interface height and (b) flow pattern on the interface for the modified aluminium reduce cell model with flow induced electric current.

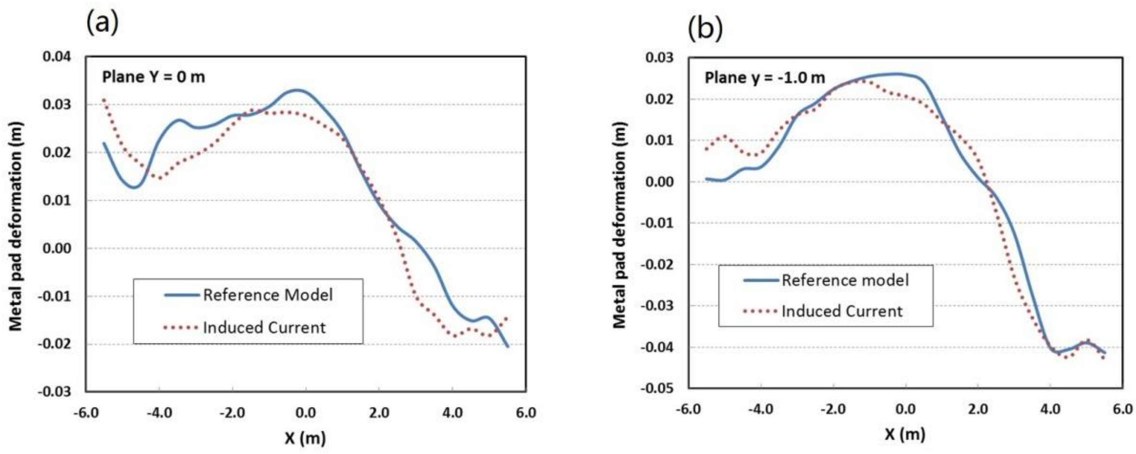

Figure 12: Comparison of the metal pad deformation along (a) the central channel y = 0 m and (b) the cell long side section y = -1.0 m under the effect of the induced current due to conductive melts flows in magnetic field.

4.4 Effect of inside cell current induced magnetic field

In order to investigate the effect of the electric current density flowing inside the reduction cell, a simulation test is conducted to take into account the magnetic field contribution due to the current density inside the cell. The rest of the model settings are the same as those in the reference case. The distribution of background magnetic flux density ($\mathbf{B}_o$) at the horizontal plane (z = 0.1 m) is shown in Figure 13(a), and the distribution of the induced magnetic flux density ($\mathbf{B}_i$) due to the cell-inside current is shown in Figure 13(b). The distribution of the induced magnetic flux density follows the pattern of background magnetic field closely, but its magnitude is about one tenth of that of the background magnetic field. The predicted bath-metal deformation and flow pattern are shown in Figure 14. Compared with predictions of the reference model, the differences are very small. Detailed comparisons of metal pad deformation (averaged from t = 140 s to t = 200 s) along the cell central channel (y = 0 m) and the cell long side section (y = -1.0 m) predicted by the current model and the reference model is shown in Figure 15. The metal pad deformation predicted by the current model is very close to the reference model. Hence, it can be concluded that the magnetic field due to the current density inside the cell has a minor effect on the metal pad deformation.

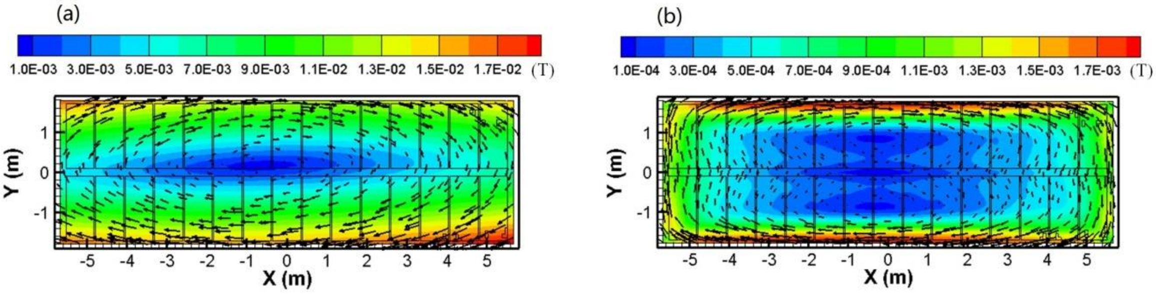

Figure 13: Distributions of (a) background magnetic flux density and (b) cell inside electric current induced magnetic flux density at the horizontal plan of z = 0.1m.

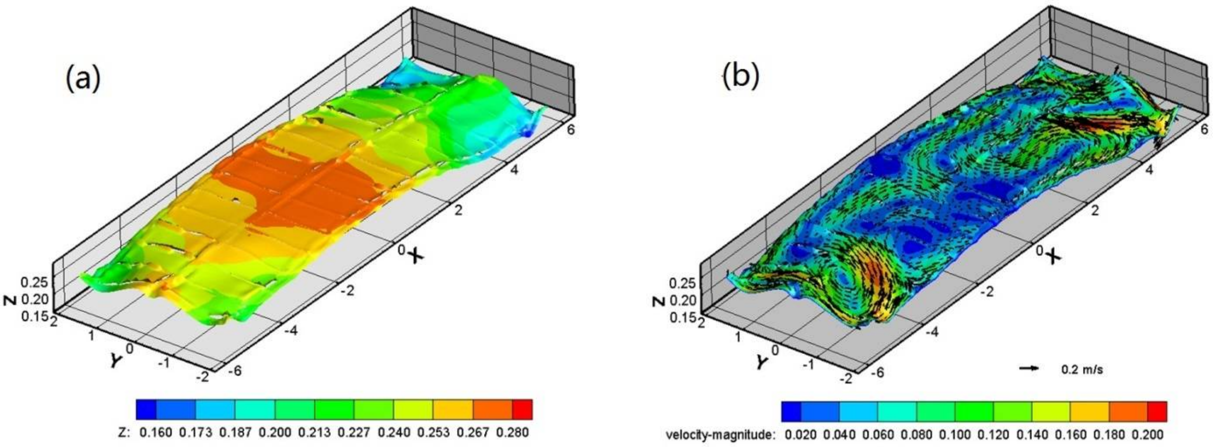

Figure 14: Predicted (a) bath-metal interface height and (b) flow pattern on the interface for the modified aluminium reduce cell model with induced magnetic field.

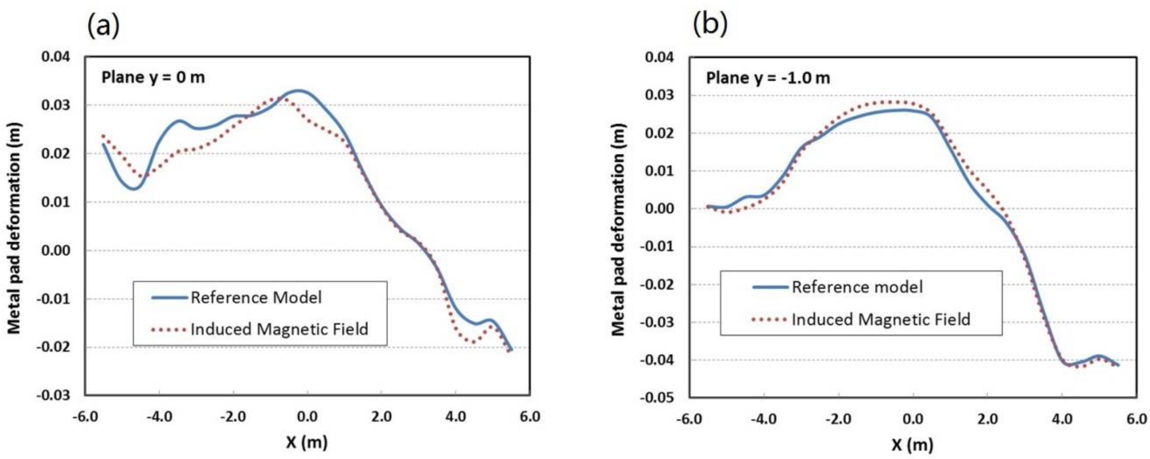

Figure 15: Comparison of the metal pad deformation along (a) the central channel y = 0 m and (b) the cell long side section y = -1.0 m under the effect of cell inside electric current induced magnetic field.

4.5 Effect of side ledge profile

In order to understand the effects of the ledge profile, we conducted two more simulations: one based on a box cell model [15] and the other based on the modified reference model, with the extended ledge profile as shown in Figure 2. The concept of box cell model was used in many early studies [7] to simplify the complex cell geometry. Figure 16 shows (a) the predicted metal pad deformation and (b) the flow pattern on the bath-metal interface. When they are compared to the results of the reference model shown in Figures 6(f) and 7(f), it is clear that the box cell model over predicts the metal heaving deformation and produces much stronger circulating flows in the cell corners, which deviates from the realistic scenario. This shows that simplifications of cell geometry may lead to significant errors in the metal pad deformation predictions.

Figure 17 shows the simulation results for the modified reference cell model with the extended ledge profile for the long side only. Compared to those of the reference model, the metal pad heaving amplitude is smaller, the flow pattern on the bath-metal interface is changed, and the flow speed is lower. The slanted angle of side walls [11] or the ledge profiles can affect the directions of Lorentz force and the liquid flow near the cell sidewall, and finally the flow pattern in the whole aluminium reduction cell.

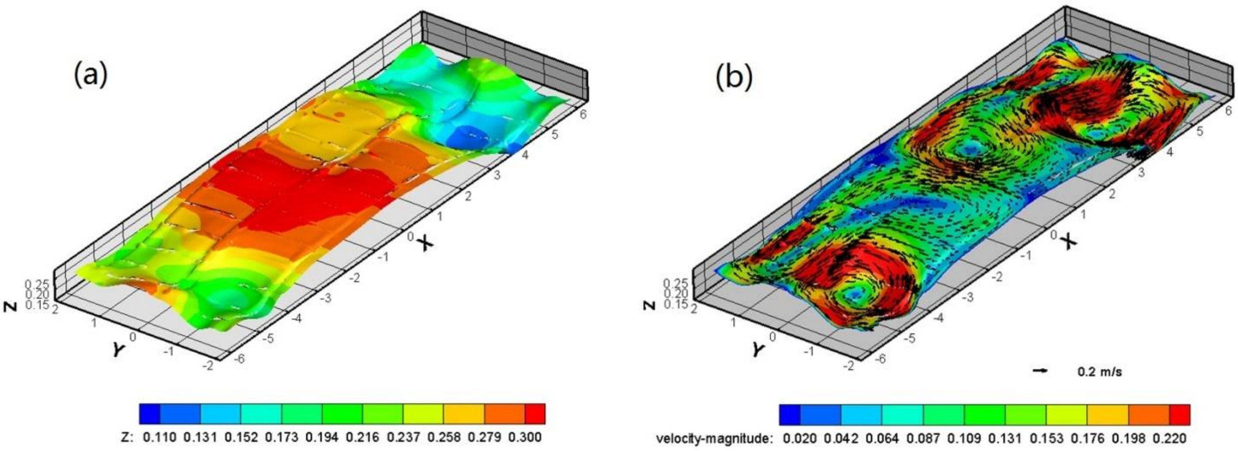

Figure 16: Predicted (a) bath-metal interface height and (b) flow pattern on the interface for the box cell model, where the ledge profile is assumed to be vertical.

A comparison of the metal pad deformation (averaged from t = 140 s to t = 200 s) along the central plane (y = 0 m) and the long side plane (y = -1.0 m) for the different ledge profiles is shown in Figure 18. The ledge profile affects the metal pad deformation [11] significantly, especially when the cell sidewall is changed from a nearly vertical wall to an inclined wall. In other words, the metal pad heaving and flow pattern inside the aluminium reduction cells can be adjusted by controlling the ledge profile. The ledge profile can possibly be changed by introducing a side wall inclination or controlling the heat loss rate on the side wall.

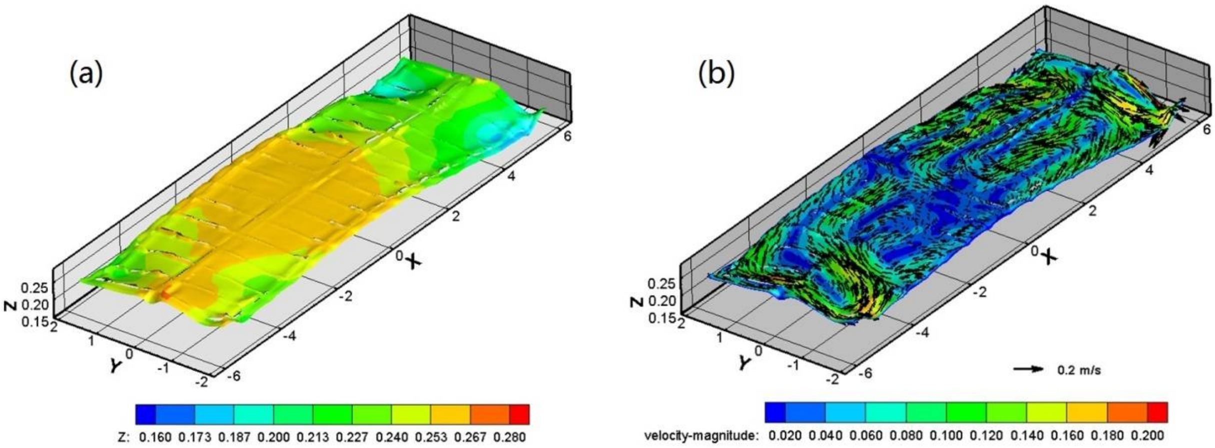

Figure 17: Predicted (a) bath-metal interface height and (b) flow pattern on the interface for the modified aluminium reduce cell model with extended side ledge profile.

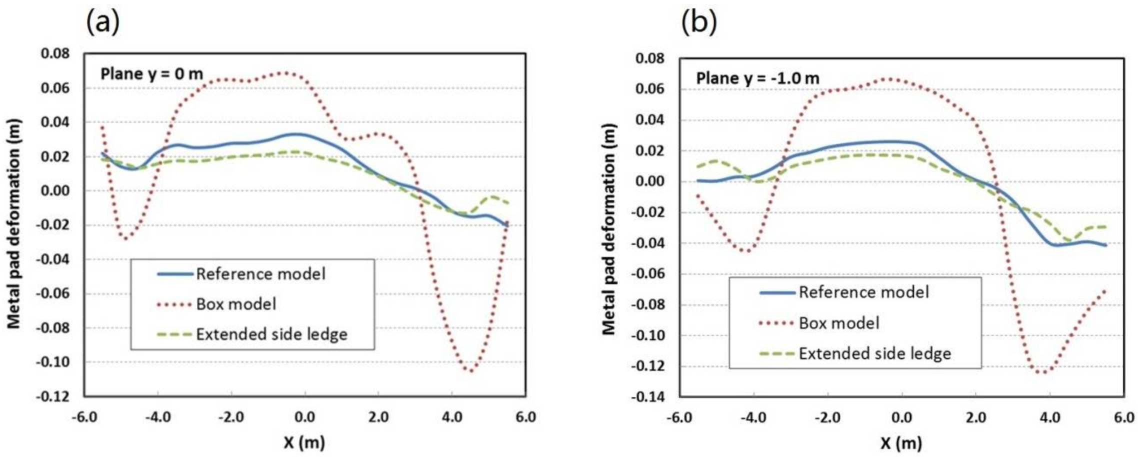

Figure 18: Comparison of the metal pad deformation along (a) the central channel y = 0 m and (b) the cell long side section y = -1.0 m under different side ledge profiles

4.6 Effect of cross-channel

It is believed that the cross-channels, the small gap between the adjacent anodes along the cell transverse direction, plays an important role on the release of gas bubbles generated at the anode bottom [18, 19]. However, its contribution to the hydraulic balance inside the reduction cell [20] is not highlighted in the previous studies. Figure 19 shows the predictions of an artificial cell model modified from the reference model by ignoring the cross-channels. When they are compared to the results of the reference model, it is found that the steady dome-shaped metal pad is no longer reproduced. Instead, a wavy bath-metal interface is found as shown in Figure 19(a). The transient variations of metal pad height distribution with time are shown in Figure 20. The bath-metal interface becomes unstable when ignoring the cross-channels.

On the other hand, the effect of increased cross-channel width is studied in another simulation test by doubling the cross-channel width of the reference model. The simulation results shown in Figure 21 indicate that quasi-steady metal pad and flow pattern are obtained, and are very similar to those of the reference model.

A comparison of metal pad deformation (averaged from t = 140 s to t = 200 s) along the cell central plane (y = 0 m) and the side plane (y = -1.0 m) for different cross-channel widths is shown in Figure 22. The overall distribution of metal pad deformation over the long axis of the reduction cell (along the central channel) is less dependent on the cross-channel width. Even if the transient metal pad becomes wavy and unstable when the cross-channel is neglected, the averaged metal pad profile still follows the overall metal pad deformation pattern. In addition, a close study of Figure 21 indicates that the larger cross-channel width can induce slightly smaller metal pad deformation. This indicates that the cross-channels contribute effectively to the hydraulic balance inside the reduction cell and stabilize the bath-metal interface. In the recent novel anode design, slots are introduced at the anode bottom [18, 19]. These slots will not only make the release of gas bubble easier, but also enhance the bath-metal interface stability, which may result in higher cell energy efficiency.

As we noted, the cross-channels were neglected in some previous numerical models to simplify the cell geometry [3, 7]. It should be highlighted that this simplification may cause significant error in the model predictions.

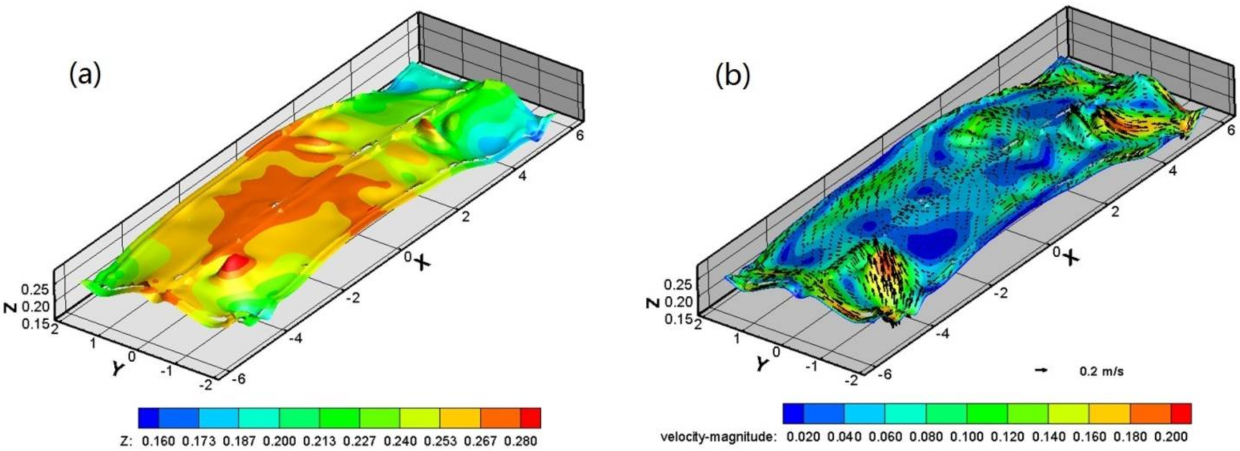

Figure 19: Predicted (a) bath-metal interface height and (b) flow pattern on the interface for the modified aluminium reduce cell model without cross-channels.

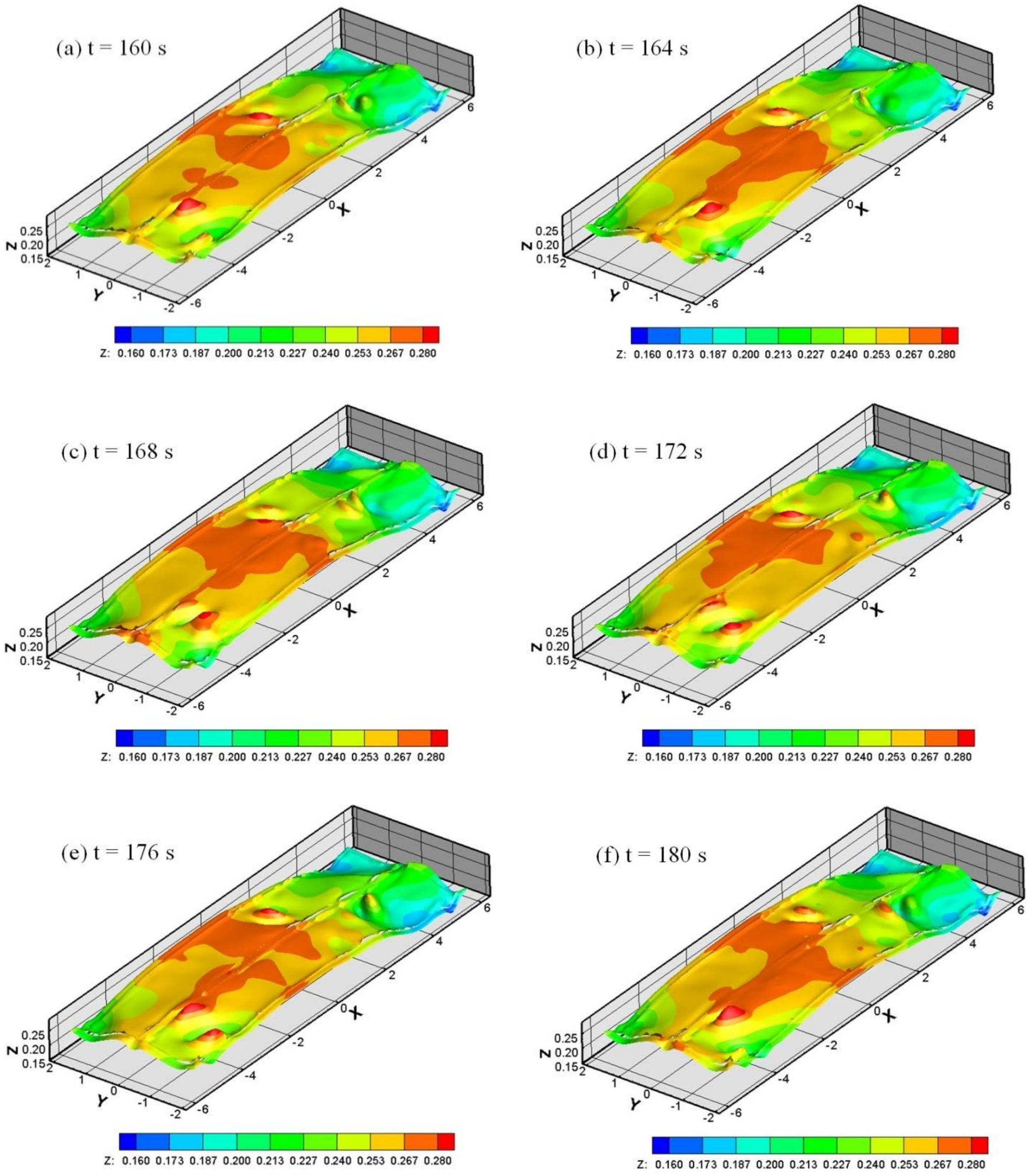

Figure 20: Predicted temporal variation of bath-metal interface height by the model ignoring the cross-channels. Local waves on the interface are predicted.

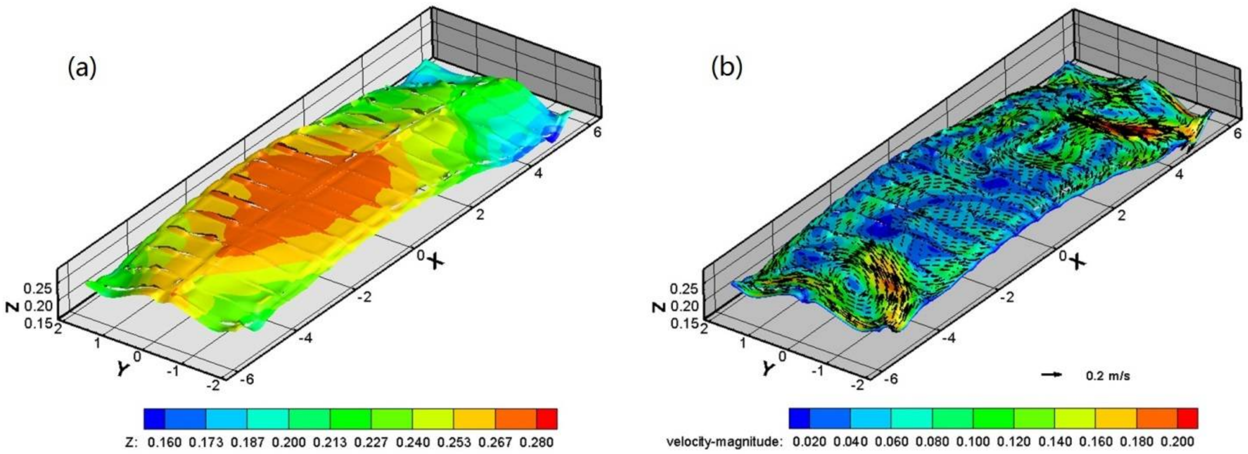

Figure 21: Predicted (a) bath-metal interface height and (b) flow pattern on the interface for the modified aluminium reduce cell model with doubled cross-channel width.

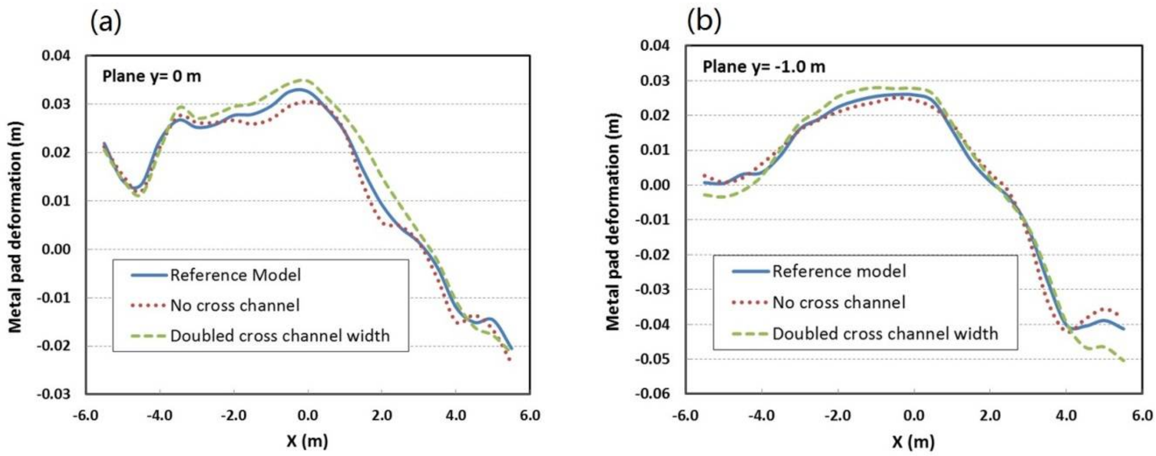

Figure 22: Comparison of the metal pad deformation along (a) the central channel y = 0 m and (b) the cell long side section y = -1.0 m under effect of cross-channel width.

4.7 Effect of anode cathode distance (ACD)

It is clear that the energy consumption in aluminium electrolysis process can be reduced by minimizing the ACD. Hence, it is also important to understand the effect of the ACD on the melt flow and the metal pad deformation. Modified from the basic settings of the reference model (ACD = 4 cm), the ACD in the two additional simulations is set to be 6 cm and 8 cm respectively. The new simulations show that the ACD have a minor effect on the simulation results when the anode cathode distance is high (ACD = 6 cm or ACD = 8 cm). Figure 23 shows the predicted metal pad deformation and the liquid flow pattern on the interface when ACD is 6 cm. Compared with the results of the reference model (ACD = 4 cm), the smaller ACD leads to higher metal pad heaving amplitude.

Detailed comparison of metal pad deformation (averaged from t = 140 s to t = 200 s) along the cell central plane (y = 0 m) and the side plane (y = -1.0 m) for the mentioned ACDs is shown in Figure 24. It shows that smaller ACD can lead to larger metal pad deformation and more fluctuations. This means that it will be more challenging to maintain the bath-metal interface stability and the high cell energy efficiency when the ACD is minimized.

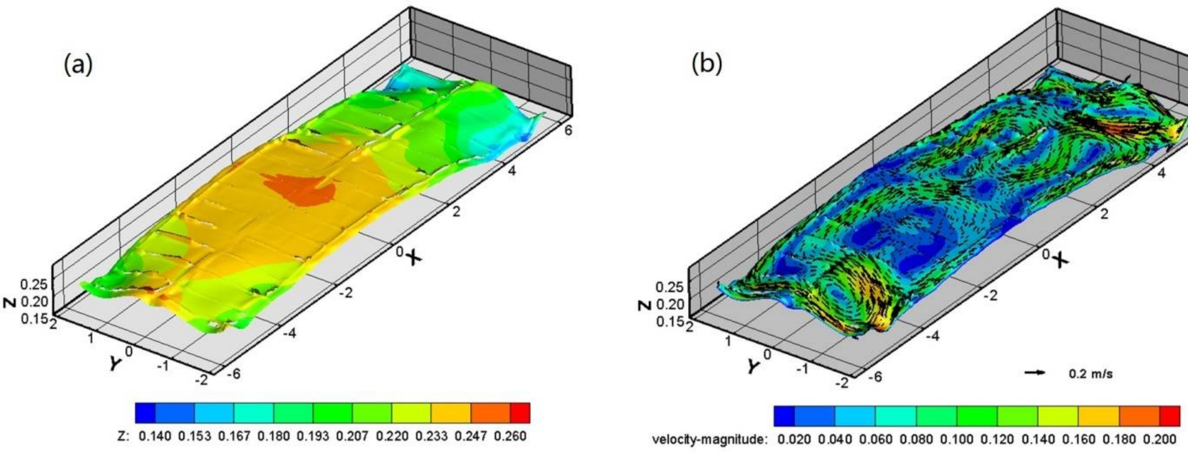

Figure 23: Predicted (a) bath-metal interface height and (b) flow pattern on the interface for the modified aluminium reduce cell model with larger ACD = 6 cm.

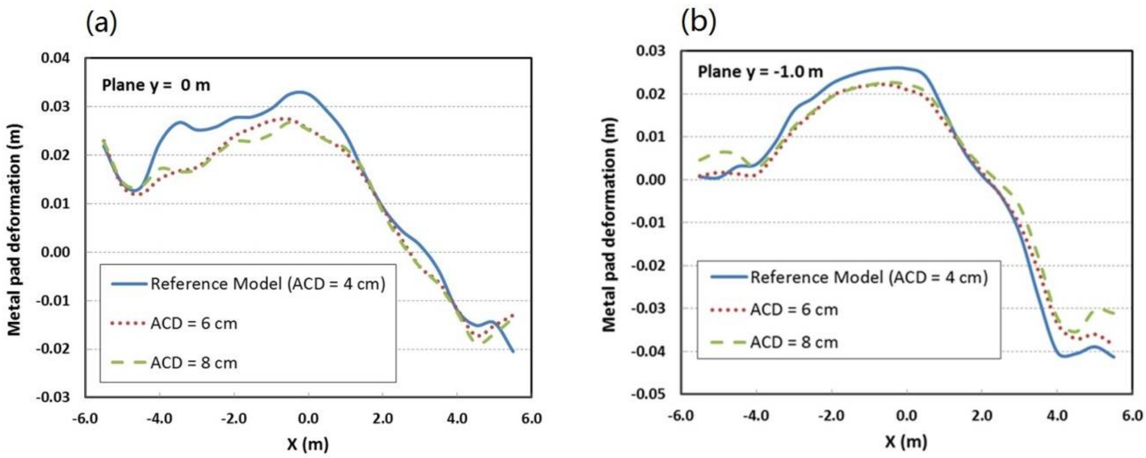

Figure 24: Comparison of the metal pad deformation along (a) the central channel y = 0 m and (b) the cell long side section y = -1.0 m under the effect of ACD.

4.8 *Effect of current distribution on cathode*

Certainly, the electric current distribution inside the reduction cell contributes directly to the Lorentz force field which significantly affects the melt flow field, the metal pad deformation and the bath-metal interface stability. The electric current distribution in an aluminium reduction cell is closely related to the cathode design. Recently, some novel cathode designs [12, 13, 14] are made with the aim to improve the metal pad stability and to lower ACD in order to reduce energy consumption. In the present model, the cathode model is not included directly in the simulation. For the reference model, the normal current density at the cathode top surface is specified according to the results of an in house electromagnetic model. In order to understand effects of cathode current distribution on the melts flow and metal pad stability, two artificial current density profiles (Profiles B and C) shown in Figure 5 are tested. The current density profile B has more non-uniform distribution in the transverse direction, high current near side and low current density at center. On the contrary, the current density profile C has more uniform distribution, which implies that more current flows vertically with smaller horizontal components. Figure 25 shows the predicted bath-metal interface height distribution and melts flow pattern on the interface when the current density profile B is set on the cathode top, and Figure 26 shows the results when the current density profile C is set. Comparison of the results, illustrated in Figures 25 and 26, shows that a higher non-uniformity in the current density, at the cathode top, results in a larger metal pad deformation. Figure 27 shows the detailed comparison of metal pad deformation (averaged from t = 140 s to t = 200 s) along the cell central plane y = 0 m and the side plane y = -1.0 m for various applied current density profiles. A more uniform current density distribution leads to a smaller metal pad deformation because the difference of the electromagnetic forces in the bath and metal layers becomes smaller.

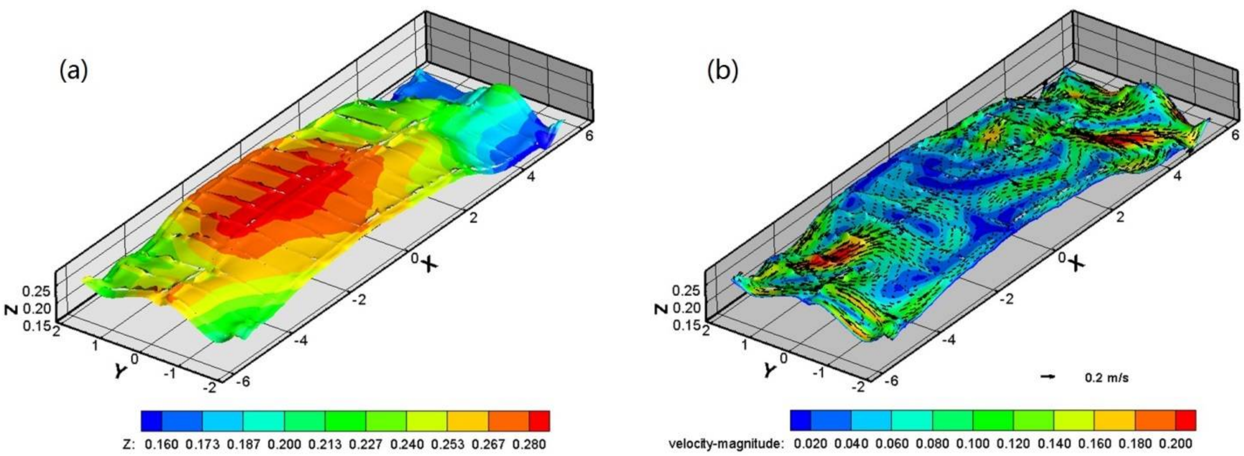

Figure 25: Predicted (a) bath-metal interface height and (b) flow pattern on the interface for the modified aluminium reduce cell model with highly non-uniform distribution of current density (profile B) on cathode surface.

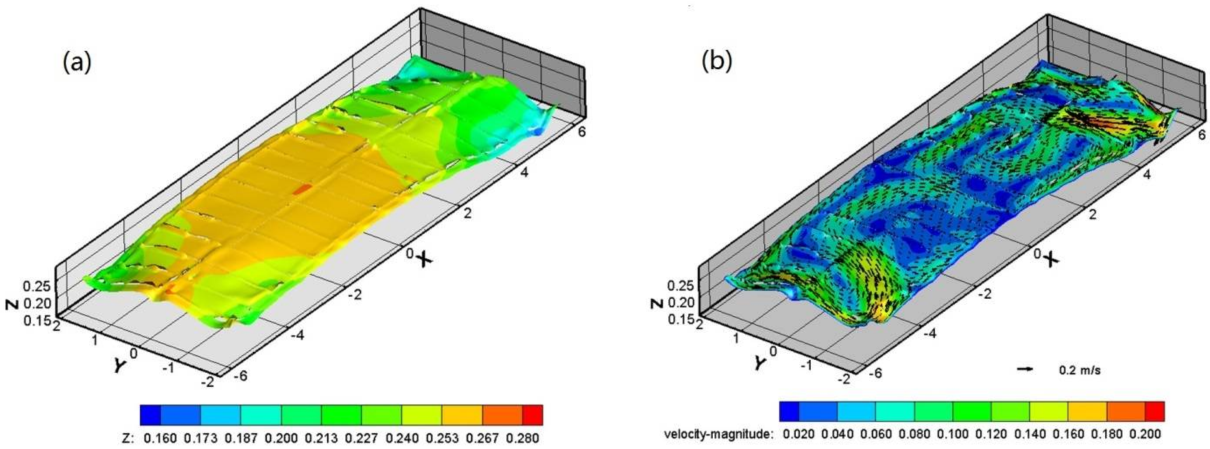

Figure 26: Predicted (a) bath-metal interface height and (b) flow pattern on the interface for the modified aluminium reduce cell model with relatively uniform distribution of current density (profile C) on cathode surface.

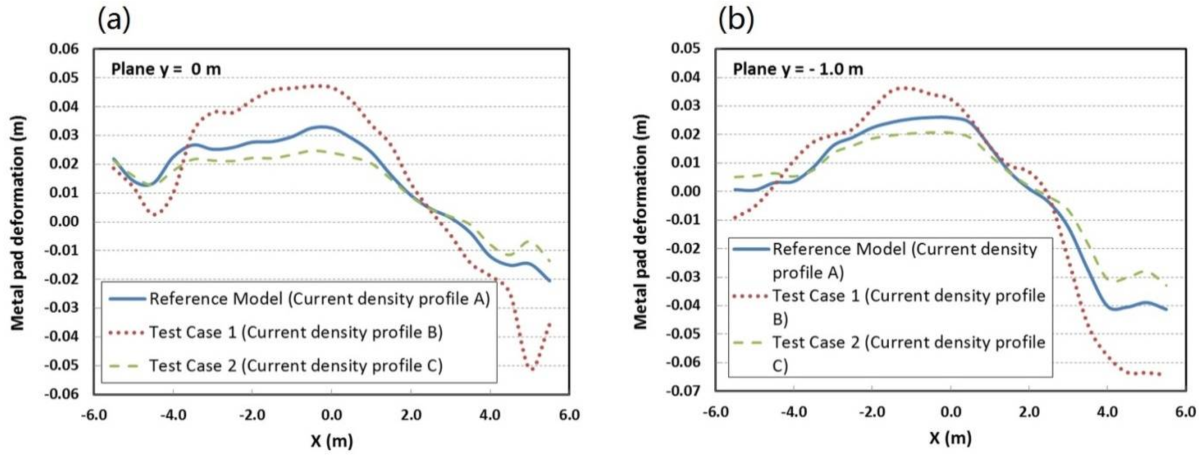

Figure 27: Comparison of the metal pad deformation along (a) the central channel y = 0 m and (b) the cell long side section y = -1.0 m under the effect of current density distribution on the cathode surface.

4.9 Effect of open channel top

In cell operation, the top of bath layer is open to the ambient environment at the channels when the top frozen crust is broken at some spots for feeding alumina. To take this into consideration, the boundary condition at the channel top is modified as the pressure outlet condition so that it is open to the ambient with a constant pressure. With the updated boundary condition at channel top, the calculation for the reference model is continued for another 180 s. The results for metal pad and flow pattern from this simulation are shown in Figure 28. A quasi-steady dome shaped metal heaving is predicted. Compared to the results of the reference model, the metal pad heaving is further enhanced at the cell enter, while the metal pad is lower at the sides. The circulating flow at the cell corners becomes weaker.

A comparison of the metal pad deformation along the central channel under the effect channel top is shown in Figure 29. As reported in [7, 15], the open channel top has a significant effect on metal pad deformation. The open channel causes larger metal pad deformation in the reduction cell.

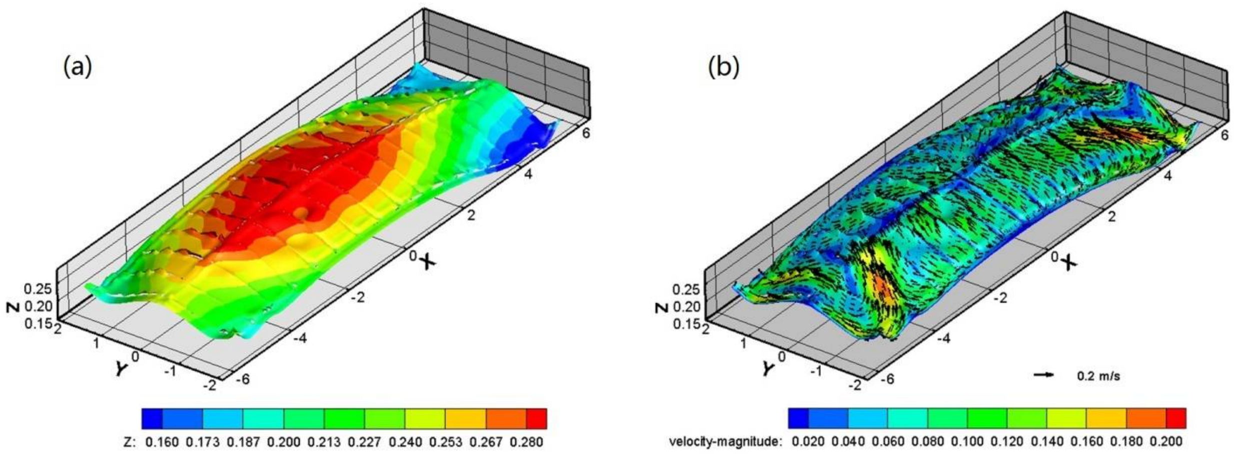

Figure 28: Predicted (a) bath-metal interface height and (b) flow pattern on the interface for the modified aluminium reduce cell model with open channel top.

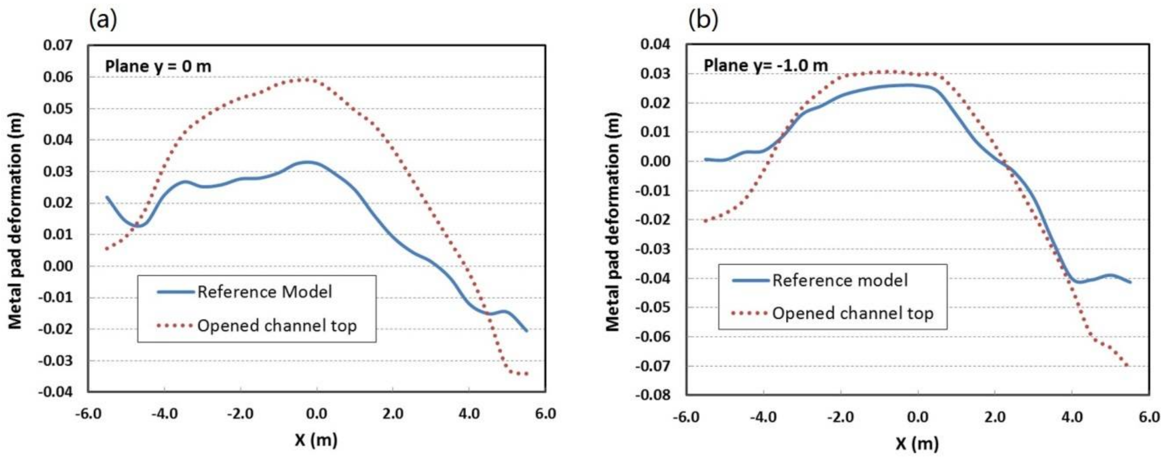

Figure 29: Comparison of the metal pad deformation along (a) the central channel y = 0 m and (b) the cell long side section y = -1.0 m under the effect of channel top openness.

5 Conclusions

A computational fluid dynamics (CFD) based multiphase magnetohydrodynamic (MHD) flow model for simulating the melt flow and metal pad heaving in realistic aluminium reduction cells is presented. The model describes the complex multiphase MHD flow problem in the aluminium electrolysis process by coupling the two-phase liquid flow, interface deformation, electric current density field, magnetic field and electromagnetic force. In addition, the model includes the geometry details of the reduction cells (e.g. ledge profile and all channels around anodes) and realistic cell operation conditions (e.g. anode consumption and constant ACD, current density profile on cathode and open channel top to ambient).

In order to investigate the model sensitivity and evaluate the model performance, a number of simulation tests with various settings (physics, cell geometry and operation conditions) were conducted. The simulation results are compared with those of the reference model. The assumption of a flat bath-metal interface and the simplification of the reduction cell as a rectangular box, which are common in the previous models, can introduce significant errors in estimating the melt flow pattern and metal pad deformation. The induced electric current density by the flowing conductive liquid in the magnetic field shows an effect on metal pad deformation at the longitudinal ends of the reduction cell, while the induced magnetic field due to the electric current density inside the cell shows a minor effect. Smaller ACD may lead to larger metal pad deformation and more fluctuations on the bath-metal interface. The cross-channels (the transverse gap between anodes or anode slots) play an important role in stabilizing the bath-metal interface. The ledge profile, the current density distribution on cathode top and open channel top also affect the metal pad deformation significantly. These factors may be tuned in the cell design to optimize the cell operation conditions for high energy efficiency. The current model may serve as an efficient numerical tool for industrial optimization of the aluminium reduction cell design and operation.

The wide range of simulations including the most relevant parameters shows that the current modelling approach is generic and reliable in predicting the metal pad heaving and melts flows in aluminium reduction cells. However, some aspects of modelling aluminium reduction cells are still not included in the current model, e.g. bubble flow under anode, thermal effects, anode burn-off mechanism, dynamic ledge profile and MHD waves on bath-metal interface. These are the interesting research topics for further development and extension of the model capability.

Acknowledgment

The present work was supported by several projects financed by the Research Council of Norway, Institute for Energy Technology and Hydro Primary Metal Technology.

References

[1] M. Segatz, D. Vogelsang, C. Droste, and P. Baekler: *Light Metals*, TMS, Warrendale, PA, 1993, pp. 361-368.

[2] M. Segatz, C. Droste and D. Vogelsang: *Light Metals*, TMS, Warrendale, PA, 1997, pp 429-435.

[3] O. Zikanov, A. Thess, P.A. Davidson and D.P. Ziegler: *Metall. Mater. Trans. B*, 2000, vol. 31B, pp. 1541-1550.

[4] V. Bojarevics and K. Pericleous: *Light Metals*, TMS, Warrendale, PA, 2009, pp. 569-574.

[5] V. Potocnik: *Light Metals*, TMS, Warrendale, PA, 1989, pp. 227-235.

[6] D.S. Severo, A.F. Schneider, E.C.V. Pinto, V. Gusberti and V. Potocnik: Light Metals, TMS, Warrendale, PA, 2005, pp. 475–480.

[7] D.S. Severo, V. Gusberti, A.F. Schneider, E.C.V. Pinto and V. Potocnik: Light Metals, TMS, Warrendale, PA, 2008, pp. 413-418.

[8] J.F. Gerbeau, T. Lelièvre, and C. Le Bris: *J. Comput. Phys.*, 2003, vol. 184, pp. 163-191.

[9] D. Munger and A. Vincent: *J. Comput. Phys.*, 2006, vol. 217, pp. 295-311.

[10] J. Li, Y. Xu, H. Zhang and Y. Lai: *Int. J. Multiphase Flow*, 2011, vol. 37, pp. 46-54.

[11] S. Das, G. Brooks and Y. Morsi: *Metall. Mater. Trans. B*, 2011, vol. 42B, pp. 243-253.

[12] S. Das, Y. Morsi, G. Brooks, Cathode characterization with steel and copper collector bars in an electrolytic cell. JOM, 2014, vol. 66, pp. 235-244.

[13] Q. Wang, B. Li, Z. He and N. Feng: *Metall. Mater. Trans. B*, 2014, Vol. 45B, pp. 272-294.

[14] Y. Song, J. Peng, Y. Di, Y. Wang, B. Li and N. Feng, *JOM*, 2015, vol. 68, pp. 593-599.

[15] J. Hua, C. Droste, K.E. Einarsrud, M. Rudshaug, R. Jorgensen and N.-H. Giskeodegard: Light Metals, TMS, Warrendale, PA, 2014, pp. 691-695.

[16] J. Hua, M. Rudshaug, C. Droste, R. Jorgensen and N.-H. Giskeodegard: Light Metals, TMS, Warrendale, PA, 2016, pp. 339-344.

[17] S. B. Pope, Turbulent Flows, Cambridge University Press, 2000.

[18] H.P. Dias and R. R. de Moura: Light Metals, TMS, Warrendale, PA, 2005, pp. 341-346.

[19] D.S. Severo, V.Gusberti, E.C.V. Pinto and R.R. Moura: Light Metals, TMS, Warrendale, PA, 2007, pp. 287-292.

[20] J. P. Givry: *Trans. Met. Soc.* AIME, 1967 vol. 239, pp. 1161-1166.

Figures and Tables

Table 1: Material Properties used for metal pad model.

Figure 1: Vertical cut of a Hall-Héroult cell.

Figure 2: (a) An overview of the model for a realistic reference alumina reduction cell, (b) a zoom view of the CFD model about ledge profile and deformed anode bottom.

Figure 3: Modelling strategy to maintain constant anode cathode distance (ACD) by relocating the anode bottom mesh grids according to the deformed bath-metal interface.

Figure 4: (a) Ledge profiles for the long side of the reference model and for a test model to investigate its significance; (b) Ledge profile for the short side of the reference model.

Figure 5: Electric current density profiles on the cathode surface.

Figure 6: Predicted temporal variation of bath-metal interface height for the reference aluminium reduction cell.

Figure 7: Predicted temporal variation of flow pattern on the bath- metal interface for the reference aluminium reduction cell.

Figure 8: Distribution of Lorentz force on the horizontal plane Z= 0.2m at the quasi-steady state.

Figure 9: (a) Predicted flow pattern on the bath- metal interface and (b) estimated metal pad heaving for an aluminium reduction cell model with the assumption of flat bath-metal interface.

Figure 10: Distributions of (a) total current magnitude and (b) flow induced electric current magnitude at the horizontal plan of z = 0.1m at the quasi-steady state.

Figure 11: Predicted (a) bath-metal interface height and (b) flow pattern on the interface for the modified aluminium reduce cell model with flow induced electric current.

Figure 12: Comparison of the metal pad deformation along (a) the central channel y = 0 m and (b) the cell long side section y = -1.0 m under the effect of the induced current due to conductive melts flows in magnetic field.

Figure 13: Distributions of (a) background magnetic flux density and (b) cell inside electric current induced magnetic flux density at the horizontal plan of z = 0.1m at the quasi-steady state.

Figure 14: Predicted (a) bath-metal interface height and (b) flow pattern on the interface for the modified aluminium reduce cell model with induced magnetic field.

Figure 15: Comparison of the metal pad deformation along (a) the central channel y = 0 m and (b) the cell long side section y = -1.0 m under the effect of cell inside electric current induced magnetic field.

Figure 16: Predicted (a) bath-metal interface height and (b) flow pattern on the interface for the box cell model, where the ledge profile is assumed to be vertical.

Figure 17: Predicted (a) bath-metal interface height and (b) flow pattern on the interface for the modified aluminium reduce cell model with extended side ledge profile.

Figure 18: Comparison of the metal pad deformation along (a) the central channel y = 0 m and (b) the cell long side section y = -1.0 m under different side ledge profiles.

Figure 19: Predicted (a) bath-metal interface height and (b) flow pattern on the interface for the modified aluminium reduce cell model without cross-channels.

Figure 20: Predicted temporal variation of bath-metal interface height by the model ignoring the cross-channels. Local waves on the interface are predicted.

Figure 21: Predicted (a) bath-metal interface height and (b) flow pattern on the interface for the modified aluminium reduce cell model with doubled cross-channel width.

Figure 22: Comparison of the metal pad deformation along (a) the central channel y = 0 m and (b) the cell long side section y = -1.0 m under effect of cross-channel width.

Figure 23: Predicted (a) bath-metal interface height and (b) flow pattern on the interface for the modified aluminium reduce cell model with larger ACD = 6 cm.

Figure 24: Comparison of the metal pad deformation along (a) the central channel y = 0 m and (b) the cell long side section y = -1.0 m under the effect of ACD.

Figure 25: Predicted (a) bath-metal interface height and (b) flow pattern on the interface for the modified aluminium reduce cell model with highly non-uniform distribution of current density (profile B) on cathode surface.

Figure 26: Predicted (a) bath-metal interface height and (b) flow pattern on the interface for the modified aluminium reduce cell model with relatively uniform distribution of current density (profile C) on cathode surface.

Figure 27: Comparison of the metal pad deformation along (a) the central channel y = 0 m and (b) the cell long side section y = -1.0 m under the effect of current density distribution on the cathode surface.

Figure 28: Predicted (a) bath-metal interface height and (b) flow pattern on the interface for the modified aluminium reduce cell model with open channel top.

Figure 29: Comparison of the metal pad deformation along (a) the central channel y = 0 m and (b) the cell long side section y = -1.0 m under the effect of channel top openness.

Table 1: Material Properties used for metal pad model.

Material property	Unit	Electrolyte	Liquid Aluminium
Density	kg/m^3	2070	2270
Viscosity	mPa s	1.25	2.5
El. conductivity	$S\ m^{-1}$	250	3.0E6